

## Photocatalytic Degradation of Methylene Blue in Presence of Graphene Oxide/TiO<sub>2</sub> Nanocomposites

Sung Phil Kim and Hyun Chul Choi\*

Department of Chemistry and Institute of Basic Science, Chonnam National University, Gwangju 500-757, Korea

\*E-mail: chc12@chonnam.ac.kr

Received April 22, 2014, Accepted May 7, 2014

A simple method of depositing titanium dioxide (TiO<sub>2</sub>) nanoparticles onto graphene oxide (GO) as a catalytic support was devised for photocatalytic degradation of methylene blue (MB). Thiol groups were utilized as linkers to secure the TiO<sub>2</sub> nanoparticles. The resultant GO-supported TiO<sub>2</sub> (GO-TiO<sub>2</sub>) sample was characterized by transmission electron microscopy (TEM), near-edge X-ray absorption fine structure (NEXAFS), and X-ray photoelectron spectroscopy (XPS) measurements, revealing that the anatase TiO<sub>2</sub> nanoparticles had effectively anchored to the GO surface. In the photodegradation of MB, GO-TiO<sub>2</sub> exhibited remarkably enhanced photocatalytic efficiency compared with thiolated GO and pure TiO<sub>2</sub> nanoparticles. Moreover, after five-cycle photodegradation experiment, no obvious deactivation was observed. The overall results showed that thiolated GO provides a good support substrate and, thereby, enhances the photodegradation effectiveness of the composite photocatalyst.

**Key Words :** Thiolated graphene oxide, GO-TiO<sub>2</sub>, Photocatalyst, Methylene blue

### Introduction

Organic dyes are widely used in various industrial fields such as textiles, leather, food, plastics, and cosmetic. They are classified according to their chemical structures into different classes including azo, anthraquinone, indigoide, phthalocyanine, sulphur, triphenylmethane, polymeric, and heterocyclic derivatives.<sup>1,2</sup> Unfortunately, organic dye and dyestuffs can cause serious environmental problems due to their high toxicity to aquatic creatures and carcinogenic and mutagenic effects on humans.<sup>3,4</sup> Moreover, they can also partially or fully prevent sunlight's penetration into water, leading eventually to the destruction of an aquatic ecosystem. Therefore, removal of organic dyes from industrial effluents is a technological goal of considerable importance. Conventional physicochemical and biological treatment methods are ineffective, due to most dyes' complex aromatic structure rendering them more stable and thus difficult to biodegrade. In response to this dilemma, many alternative removal processes have been proposed over the years. Semiconductor-assisted photocatalysis, for example, recently has emerged as an organic pollutant degradation and decolorization method.<sup>5,6</sup>

Titanium dioxide (TiO<sub>2</sub>) is one of the most promising photocatalysts for environmental purification purposes, owing specifically to its high efficiency, low toxicity, excellent physical and chemical stability, and low cost.<sup>7-9</sup> When TiO<sub>2</sub> nanoparticles are illuminated with ultraviolet (UV) light, electron/hole pairs are generated. These electrons and holes can migrate and initiate redox reactions with water and oxygen, by which they degrade organic molecules absorbed on the surface of a photocatalyst. The overall efficiency of TiO<sub>2</sub> is greatly influenced by crystal structure, particle size,

surface area, and porosity. One of the strategies for improved photocatalytic efficiency entails the use of nano-sized TiO<sub>2</sub>.<sup>10-12</sup> However, the applications of TiO<sub>2</sub> nanoparticles remain limited by drawbacks such as a higher recombination rate of photo-generated electron/hole pairs, a lower solar-energy absorption utility due to their wide band gap, and the difficulty of their post-photocatalysis separation and recycling from a reaction system. In this regard, immobilization of nano-sized TiO<sub>2</sub> onto insoluble supports has become a popular approach to the preparation of high-efficiency photocatalysts.<sup>13-15</sup>

Graphene currently is receiving considerable attention as a solid support for various applications including photocatalysis, electrocatalysis, fuel cells, and solar cells, due to its high mechanical strength, large theoretical surface area (~2,600 m<sup>2</sup>/g), good electrical conductivity, and durability under harsh conditions.<sup>16,17</sup> Some researchers have reported graphene-supported catalysts that exhibit good photocatalytic behaviors for various organic pollutants including methylene blue, methyl orange, Rhodamine B, and *p*-chlorophenol.<sup>18-21</sup> Enhanced catalytic performance is generally attributed to the suppression of photocatalysts' electron/hole recombination and the increase in the number of surface-adsorbed chemical molecules through π-π interactions. However, the agglomerative property and poor solubility of graphene in water or polar organic solvents complicate the deposition of nano-sized catalysts on its surface. Graphene oxide (GO), consisting of a sheet-like graphene framework with reactive oxygen functional groups and defects, is one of the most important derivatives of graphene. The presence of such hydrophilic groups and defects makes GO an excellent support for anchoring of nano-sized catalysts and for good dispersion in aqueous solution. Recently, some researchers

have reported a superior photocatalytic efficiency for GO-supported TiO<sub>2</sub> compared with pure TiO<sub>2</sub> particles.<sup>22-26</sup> In this paper, we report a simple and effective process for preparation of GO-supported TiO<sub>2</sub> (GO-TiO<sub>2</sub>) using thiolated GO as an efficient photocatalyst for photodegradation of methylene blue (MB), a model dye contaminant commonly employed in evaluations of photocatalytic activity.

## Experimental

### Preparation of Catalysts.

**Chemicals:** Graphite powder (<20 µm), potassium persulfate (K<sub>2</sub>S<sub>2</sub>O<sub>8</sub>, 99.99%), phosphorus pentoxide (P<sub>2</sub>O<sub>5</sub>, 99.99%), potassium permanganate (KMnO<sub>4</sub>, 99%), hydrogen peroxide (H<sub>2</sub>O<sub>2</sub>, 30%), titanium tetra-*n*-butoxide [Ti-(OCH<sub>2</sub>-CH<sub>2</sub>CH<sub>2</sub>CH<sub>3</sub>)<sub>4</sub>, 97%], and titanium dioxide (TiO<sub>2</sub>, 99.9%) were purchased from Sigma-Aldrich. The other reagents were of analytical grade, and were used as received without further purification. All aqueous solutions were prepared with Milli-Q water (>18.2MΩ·cm) using a Direct Q3 system (Millipore).

**Thiolated GO:** GO was prepared from graphite powder by the modified Hummers method.<sup>27,28</sup> The graphite powder (4 g) was first pre-oxidized with a solution of concentrated H<sub>2</sub>SO<sub>4</sub> (60 mL), K<sub>2</sub>S<sub>2</sub>O<sub>8</sub> (2 g), and P<sub>2</sub>O<sub>5</sub> (2 g) at 80 °C. The resulting mixture, after cooling to room temperature, was filtered and washed until the rinse-water pH became neutral. The oxidized graphite powder (2 g) was placed in cold (0 °C) concentrated H<sub>2</sub>SO<sub>4</sub> (40 mL), and KMnO<sub>4</sub> (60 g) subsequently was added under stirring in an ice-bath. The mixture was then stirred at 35 °C for 2 h, after which distilled (DI) water (92 mL) was added. Next, additional DI water (280 mL) and 30% H<sub>2</sub>O<sub>2</sub> solution (50 mL) were added to the mixture to stop the reaction. The resulting mixture was washed by repeated centrifugation and filtration with 5% HCl solution in order to remove the metal ions. Finally, drying under vacuum at 50 °C afforded the GO product. In order to synthesize thiolated GO, GO (0.5 g) and DI water (30 mL) were added to a bottle (250 mL) and ultrasonicated for 20 min. Next, NaSH (8 g) was added gradually with stirring, which mixture was then ultrasonicated for 1 h at 40 °C. Stirring was resumed and maintained for 20 h at 55 °C to produce thiol groups on the GO surfaces. The product finally was filtered and washed with DI water and dried under vacuum for 3 h at 50 °C. By reference to the X-ray photoelectron spectroscopy (XPS) spectrum in the sulfur 2p region, the thiolation was confirmed to have recorded the characteristic energy at 163 eV.

**GO-TiO<sub>2</sub>:** TiO<sub>2</sub> nanoparticles were synthesized according to the previously reported sol-gel method.<sup>29</sup> Ti(OCH<sub>2</sub>CH<sub>2</sub>-CH<sub>2</sub>CH<sub>3</sub>)<sub>4</sub> precursor (7 mL) was dissolved into 40 mL of anhydrous ethanol under vigorous stirring for about 1 h. Twenty (20) mL of anhydrous ethanol containing 3 mL of concentrated HCl and 740 µL of DI water was poured into the obtained solution under 5 h stirring. The molar ratio of H<sub>2</sub>O to titanium tetra-*n*-butoxide was 2:1. The prepared solution was then refluxed for 2 h in order to produce

anatase TiO<sub>2</sub>. In the preparation of the GO-TiO<sub>2</sub> catalysts, a thiolated GO sample (0.15 g) was dispersed into 30 mL of anhydrous ethanol by 20 min ultrasonic vibration. The prepared TiO<sub>2</sub> solution (40 mL) was then added to the GO solution under 24 h stirring. The GO-TiO<sub>2</sub> catalyst finally was obtained by centrifugation, washed with absolute ethanol, and vacuum dried at 40 °C overnight.

**Characterization and Photocatalytic Test:** Transmission electron microscopy (TEM) images were obtained with a Tecnai-F20 system operated at 200 kV. Samples for analysis were prepared on a carbon-coated Cu grid by dip-coating in dilute-appropriate solutions (~1.0 wt % solid content). Ti L<sub>II,III</sub>-edge and O K-edge near-edge X-ray absorption fine structure (NEXAFS) measurements of the TiO<sub>2</sub> nanoparticles were performed using the 8A1 (undulator U7) beam line at Pohang Light Source (PLS). The Ti L<sub>II,III</sub>-edge NEXAFS data were obtained in the total electron yield mode, recording the sample current. All of the spectra were normalized using a reference signal from a gold (Au) mesh with 90% transmission. XPS measurements were performed using a VG Multilab 2000 spectrometer (ThermoVG Scientific) with an unmonochromatized Mg K<sub>a</sub> (1253.6 eV) excitation source. The photocatalytic properties of the prepared GO-TiO<sub>2</sub> catalysts were evaluated by measuring the photodegradation of MB (C<sub>16</sub>H<sub>18</sub>N<sub>3</sub>S-Cl-3H<sub>2</sub>O) at a 0.02 mM concentration in aqueous solution. The light source was a 72 W Hg-lamp (Philips). Prior to irradiation, 8 mg of the GO-TiO<sub>2</sub> was dispersed in 24 mL of 0.02 mM MB solution, and the suspensions were magnetically stirred for 1 h in darkness in order to attain the adsorption-desorption equilibrium. Two (2) mL aliquots were sampled at given time intervals and analyzed by recording variations in the absorption band ( $\lambda_{\text{max}} = 665$  nm) in the UV-vis spectra of MB using a Varian Cary 100 UV-vis spectrophotometer.

## Results and Discussion

Figure 1(a) shows a TEM image of thiolated GO. It is clearly evident that the thiolated GO sample has a wrinkled paper-like structure consisting of ultrathin stacked sheets. Also, the thiolated GO surface is very smooth. The corresponding energy-dispersive X-ray (EDX) spectrum of the thiolated GO presents peaks corresponding to the C, O, and S elements [Fig. 1(a), inset]. The S element indicates that sulfur-containing groups (mainly thiol groups) were generated in the thiolation. In GO-TiO<sub>2</sub> [Fig. 1(b)], the nanoparticles are densely dispersed over the surface of the thiolated GO. The GO-TiO<sub>2</sub> EDX spectrum presents peaks corresponding to the C, O, Ti and Cu elements, indicating the existence of surface TiO<sub>2</sub> nanoparticles [Fig. 1(b), inset]. GO-TiO<sub>2</sub>'s lack of any S element suggests that thiolated GO's TiO<sub>2</sub> nanoparticles preferentially deposited on the sulfur-containing groups. Significantly, the high-resolution TEM image [Fig. 1(b), inset] also reveals the highly crystalline features of the TiO<sub>2</sub> nanoparticles. The *d*-spacing of their adjacent fringe is 0.35 nm, which could be indexed to the (101) plane of anatase TiO<sub>2</sub>.

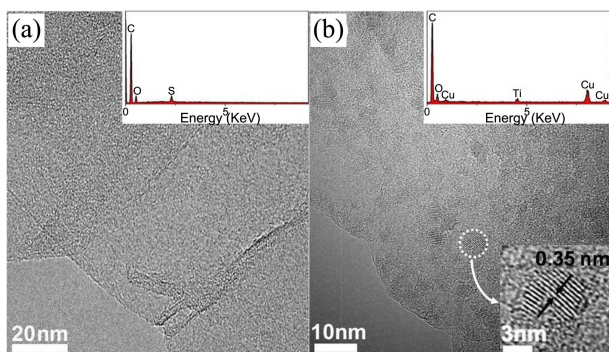


**Figure 1.** (a) Transmission electron microscopy (TEM) image of thiolated GO, with corresponding EDX spectrum (inset). (b) TEM image of GO-TiO<sub>2</sub>, with corresponding EDX spectrum and atomic-resolved image of deposited TiO<sub>2</sub> nanoparticles (inset).

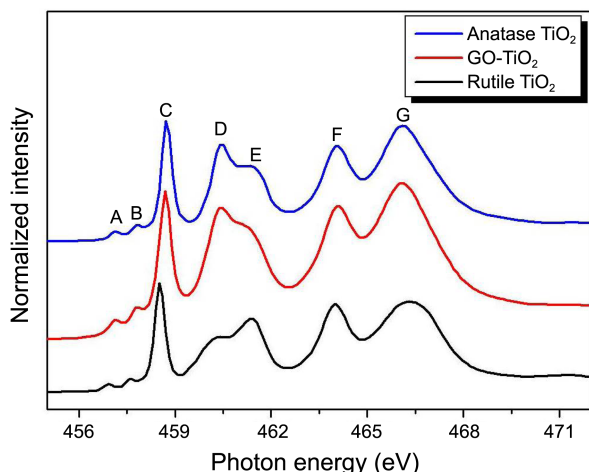


**Figure 2.** Ti L<sub>II,III</sub>-edge NEXAFS spectra of anatase TiO<sub>2</sub>, rutile TiO<sub>2</sub>, and GO-TiO<sub>2</sub>.

Figure 2 shows the Ti L<sub>II,III</sub>-edge NEXAFS spectra of the anatase TiO<sub>2</sub>, rutile TiO<sub>2</sub>, and GO-TiO<sub>2</sub>, respectively. The features of the Ti L<sub>II,III</sub>-edge spectrum can be explained by the multiplet effect, which is caused by the large Coulombic and exchange interactions of the 2p-3d and 3d-3d orbitals, and is thus directly related to the local symmetry and electron configuration of the ground state.<sup>30,31</sup> The main near-edge structure of the Ti L<sub>II,III</sub>-edge spectrum is a 2p<sup>6</sup> → 2p<sup>5</sup>g3d<sup>1</sup> dipole transition, where g is the 2p core hole. The 2p spin-orbit coupling splits the initial state into 2p<sub>3/2</sub> and 2p<sub>1/2</sub>, resulting in two L-edge features, denoted L<sub>III</sub> and L<sub>II</sub>, respectively. Both the L<sub>III</sub> and L<sub>II</sub> features further split into L<sub>III</sub>-t<sub>2g</sub>, L<sub>III</sub>-e<sub>g</sub>, L<sub>II</sub>-t<sub>2g</sub>, and L<sub>II</sub>-e<sub>g</sub> features, due to the low symmetry of the ligand field. The L<sub>III</sub>-e<sub>g</sub> feature splits into a doublet feature (peaks D and E) centered on 461 eV in NEXAFS spectra, which reflects the splitting of the e<sub>g</sub> orbitals. This splitting can be ascribed to the slight distortion of the TiO<sub>6</sub><sup>8-</sup> octahedron in the rutile and anatase structures, which results from the configurational deformation predicted by the Jahn-Teller theorem. The different polymorphs of TiO<sub>2</sub> can be distinguished by the relative intensities of the doublet features (peaks D and E). In the anatase structure,

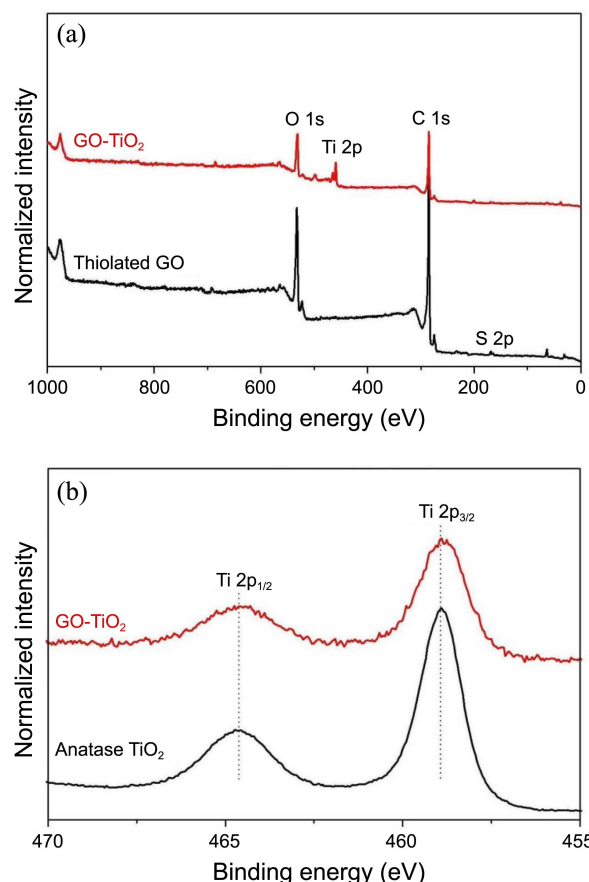


**Figure 3.** (a) XPS survey spectra of anatase TiO<sub>2</sub> and GO-TiO<sub>2</sub>. (b) Ti 2p core-level spectra of anatase TiO<sub>2</sub> and GO-TiO<sub>2</sub>.

the intensity of peak D is substantially stronger than that of peak E, whereas in the rutile structure, the opposite is the case. The spectral features of GO-TiO<sub>2</sub> confirmed the formation of the anatase structure in the prepared GO-TiO<sub>2</sub> sample. This is in good agreement with the TEM observation.

Figure 3(a) shows XPS survey spectra from the thiolated GO and GO-TiO<sub>2</sub>. For the thiolated GO, the XPS data shows distinct O 1S, C 1s and S 2p peaks, with no other elements detected. The relative surface atomic ratio was estimated from the corresponding peak areas, and was corrected with the tabulated sensitivity factors. The estimated value of the S content was about 3.4 atomic %. Since the XPS signal is obtained by collection of photo-emitted electrons, this technique is very sensitive to the surface properties. For the GO-TiO<sub>2</sub>, the photo-emitted electrons from the S atoms were screened by the deposited TiO<sub>2</sub> nanoparticles, which resulted in the featureless S 2p profile. The XPS data also confirmed the presence of Ti in the sample, the value of which content was estimated to be 5.8 atomic %. Figure 3(b) shows the Ti 2p XPS spectra for pure anatase TiO<sub>2</sub> and GO-TiO<sub>2</sub>. The binding energies, 458.9 eV for Ti 2p<sub>3/2</sub> and 464.6 eV for Ti 2p<sub>1/2</sub>, are in accordance with those of the reference anatase TiO<sub>2</sub>. Some researchers have reported that the positions of Ti 2p signals relative to those of pure anatase shift slightly toward higher binding energy, due to the forma-

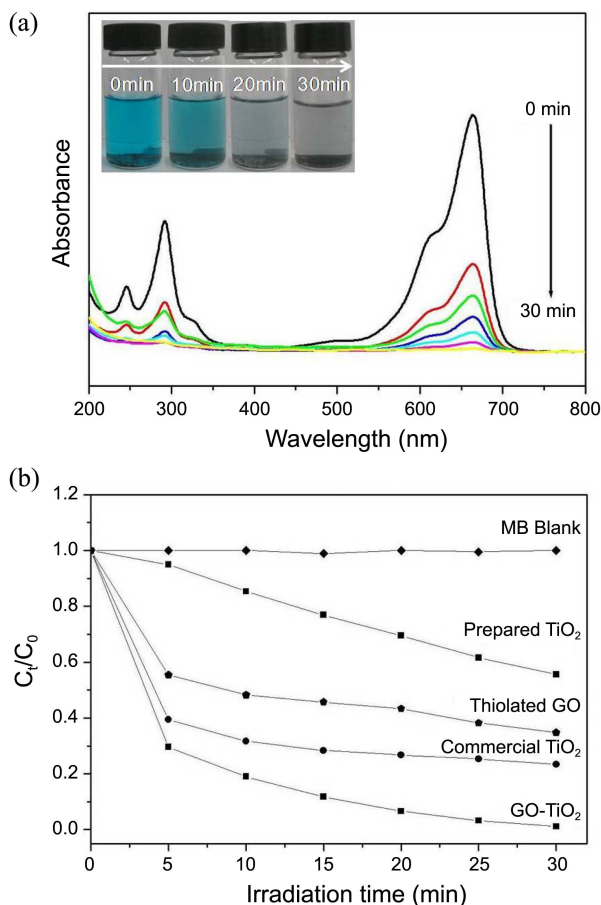


**Figure 4.** (a) Variation of UV-visible spectra of MB solution in presence of GO-TiO<sub>2</sub> catalyst under UV-vis irradiation, with corresponding MB solution color-change sequence (inset). (b) Photocatalytic degradation of MB by different photocatalysts under UV-vis irradiation.  $C_0$  is the initial concentration of MB, and  $C_t$  is the MB concentration at reaction time t.

tion of the Ti–O–C bond.<sup>32,33</sup> However, in this study, no such binding-energy shift was observed, indicating the absence of any Ti–O–C bond in the prepared GO-TiO<sub>2</sub>.

Next, the MB-degrading photocatalytic activities of the prepared GO-TiO<sub>2</sub> catalysts were evaluated under UV irradiation. Figure 4(a) plots the change in the absorption spectra of MB as a function of irradiation time in the presence of GO-TiO<sub>2</sub>. The peaks centered around 300 nm were assigned to the absorption of the aromatic ring, and the peaks between 600 and 700 nm were assigned to the absorption of the conjugated  $\pi$ -structure.<sup>34,35</sup> It was evident that the original absorption feature rapidly decreased with irradiation time and disappeared almost completely after 30 min. The lack of any new-appearing peak in the course of the reaction signaled that photodegradation had been successfully completed. To confirm the enhancement of GO-TiO<sub>2</sub>'s photocatalytic efficiency, comparative MB-photodegradation experiments were performed using prepared TiO<sub>2</sub> nanoparticles, commercial TiO<sub>2</sub>, thiolated GO, and GO-TiO<sub>2</sub>. For the purposes of comparison, MB photolysis was additionally carried out under the same conditions but without any cata-

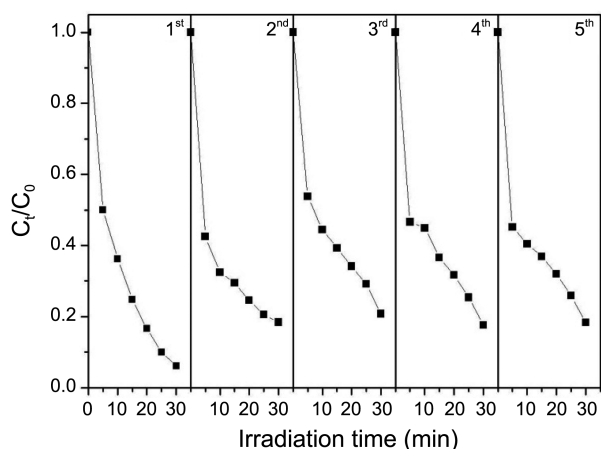


**Figure 5.** Stability testing curves of GO-TiO<sub>2</sub> over MB degradation.

lyst. The MB-degradation results for light-exposure durations ranging from 0 to 30 min are plotted in Figure 4(b). The degree of photocatalytic MB degradation as a function of time ( $C_t/C_0$ ) was calculated with respect to the maximum absorbance at 665 nm. In the “blank” test, the MB concentration, in the absence of any photocatalyst, was hardly reduced. By contrast, when the catalyst was added to the solution, noticeable MB degradation occurred: ~42, 55, 70 and 100% for the prepared TiO<sub>2</sub>, thiolated GO, commercial TiO<sub>2</sub> and GO-TiO<sub>2</sub>, respectively. These results indicated that the efficiency of the prepared TiO<sub>2</sub> catalysts was greatly enhanced by deposition on the thiolated GO surfaces. Such photocatalytic performance can be attributed to the excellent electronic conductivity and improved mass transportation, which facilitates photo-induced electron transport to the surface of the catalysts, thereby inhibiting recombination of photo-induced electrons and holes.<sup>36,37</sup> Adsorption of organic molecules also is enhanced by  $\pi$ - $\pi$  interaction between thiolated GOs and aromatic rings, thus leading to favorable reactant-product mass transportation.

Photocatalytic stability is a crucial factor in practical applications. In the present investigation, the stability of GO-TiO<sub>2</sub> was evaluated by repeating its application to the photodegradation of MB five times. As Figure 5 indicates, the activity of the GO-TiO<sub>2</sub> catalysts was diminished drastically, to about 82% of the initial value, after the five photocatalytic cycles. In these recyclings, the GO-TiO<sub>2</sub> powder could not be completely separated from the solution, resulting in continuous, per-cycle loss of activity.

## Conclusion

In summary, a hybrid GO-TiO<sub>2</sub> photocatalyst was successfully prepared by a facile two-step process. TEM observations revealed that well-dispersed TiO<sub>2</sub> nanoparticles were anchored to the surfaces of the thiolated GOs. The NEXAFS results indicated that the anatase TiO<sub>2</sub> nanoparticles also had effectively anchored to the GO surface. The estimated TiO<sub>2</sub> content in the GO-TiO<sub>2</sub> was nearly 5.8%. As for the photo-

degradation of MB, GO-TiO<sub>2</sub> exhibited a much higher photocatalytic efficiency than the prepared TiO<sub>2</sub> nanoparticles or commercial TiO<sub>2</sub>. This enhanced photocatalytic performance of GO-TiO<sub>2</sub> can be attributed to the suppression of electron recombination and the enhancement of mass transportation. Moreover, after a five-cycle photo-degradation experiment, no obvious deactivation was observed. This work demonstrates not only the potential application of GO-TiO<sub>2</sub> to organic-pollutant degradation but also the effectiveness of surface thiolation as a means of obtaining highly dispersed metal nanoparticles on GO surfaces.

**Acknowledgments.** This research was supported by the Basic Science Research Program through the National research Foundation of Korea (NRF) funded by the Ministry of Education, Science and Technology (2010-0003963). Authors thank for TEM analysis from the Korea Basic Science Institute (KBSI)-Gwangju branch in Chonnam National University.

## References

1. Carlos A, M.-H.; Brillas, E. *Appl. Catal. B-Environ.* **2009**, *87*, 105.
2. Mishra, A. K.; Arockiadoss, T.; Ramaprabhu, S. *Chem. Eng. J.* **2010**, *162*, 1026.
3. Walthal, W. K.; Stark, J. D. *Environ. Pollut.* **1999**, *104*, 207.
4. Tsuda, S.; Murakami, M.; Matsusaka, N.; Kano, K.; Taniguchi, K.; Sasaki, Y. F. *Toxicol. Sci.* **2001**, *61*, 92.
5. Hirayama, J.; Kondo, H.; Miura, Y.-K.; Abe, R.; Yuichi Kamiya, Y. *Catal. Commun.* **2012**, *20*, 99.
6. Sayama, K.; Hayashi, H.; Arai, T.; Yanagida, M.; Gunji, T.; Sugihara, H. *Appl. Catal. B-Environ.* **2010**, *94*, 150.
7. Wang, J.; Li, C.; Zhuang, H.; Zhang, J. *Food Control.* **2013**, *34*, 372.
8. Le, H. A.; Linh, L. T.; Chin, S.; Jurng, J. *Powder Technol.* **2012**, *225*, 167.
9. Wu, D.; Long, M.; Cai, W.; Chen, C.; Wu, Y. *J. Alloy. Compd.* **2010**, *502*, 289.
10. Grover, I. S.; Singh, S.; Pal, B. *Appl. Surf. Sci.* **2013**, *280*, 366.
11. Balazs, N.; Sranko, D. F.; Dombi, A.; Sipos, P.; Mogyorosi, K. *Appl. Catal. B-Environ.* **2010**, *96*, 569.
12. Lee, M. S.; Lee, G.-D.; Ju, C.-S.; Hong, S.-S. *Sol. Energy Mater. Sol. Cells* **2005**, *88*, 389.
13. Zhang, K.; Zhang, F. J.; Chen, M. L.; Oh, W. C. *Ultrason.* **Sonochem.** **2011**, *18*, 765.
14. Jiang, G.; Lin, Z.; Zhu, L.; Ding, Y.; Tang, H. *Carbon* **2010**, *48*, 3369.
15. Zhou, W.; Pan, K.; Qu, Y.; Sun, F.; Tian, C.; Ren, Z.; Tian, G.; Fu, H. *Chemosphere* **2010**, *81*, 555.
16. Antolini, E. *Appl. Catal. B-Environ.* **2012**, *123-124*, 52.
17. Wu, G.; Wang, X.; Guan, N.; Li, L. *Appl. Catal. B-Environ.* **2013**, *136-137*, 177.
18. Ismail, A. A.; Geioughy, R. A.; Bouzid, H.; Al-Sayari, S. A.; Al-Hajry, A.; Bahnmann, D. W. *Appl. Catal. B-Environ.* **2013**, *129*, 62.
19. Wang, J.; Wang, P.; Cao, Y.; Chen, J.; Li, W.; Shao, Y.; Zheng, Y.; Li, D. *Appl. Catal. B-Environ.* **2013**, *136-137*, 94.
20. Hou, Y.; Li, X.; Zhao, Q.; Chen, G. *Appl. Catal. B-Environ.* **2013**, *142-143*, 80.
21. Ghasemi, S.; Esfandiar, A.; Setayesh, S. R.; Habibi-Yangjeh, A.; Irajizad, A.; Gholami, M. R. *Appl. Catal. A-Gen.* **2013**, *462-463*, 82.
22. Gao, P.; Sun, D. D. *Appl. Catal. B-Environ.* **2014**, *147*, 888-896.
23. Pu, X.; Zhang, D.; Gao, Y.; Shao, X.; Ding, G.; Li, S.; Zhao, S. *J. Alloy. Compd.* **2013**, *551*, 382.
24. Min, Y. L.; Zhang, K.; Zhao, W.; Zheng, F. C.; Chen, Y. C.; Zhang, Y. G. *Chem. Eng. J.* **2012**, *193-194*, 203.
25. Liu, J.; Liu, L.; Bai, H.; Wang, Y.; Sun, D. D. *Appl. Catal. B-Environ.* **2011**, *106*, 76.
26. Yoo, D.-H.; Cuong, T. V.; Pham, V. H.; Chung, J. S.; Khoa, N. T.; Kim, E. J.; Hahn, S. H. *Curr. Appl. Phys.* **2011**, *11*, 805-808.
27. Kovtyukhova, N. I.; Olliver, P. J.; Martin, B. R.; Mallouk, T. E.; Chizhik, S. A.; Buzaneva, E. V.; Gorchinskii, A. D. *Chem. Mater.* **1999**, *11*, 771.
28. Kim, J. D.; Palani, T.; Kumar, M. R.; Lee, S.; Choi, H. C. *J. Mater. Chem.* **2012**, *22*, 20665.
29. Seirafianpour, N.; Badilescu, S.; Djaoued, Y.; Brüning, R.; Balaji, S.; Kahrizi, M.; Truong, V-V. *Thin Solid Films* **2008**, *516*, 6359.
30. Chen, J. G. *Surf. Sci. Rep.* **1997**, *30*, 1.
31. Lusvardi, V. S.; Barreau, M. A.; Chen, J. G.; Eng, J.; Fruhberger, B.; Teplyakov, A. *Surf. Sci.* **1998**, *397*, 237.
32. Dai, K.; Zhang, X.; Fan, K.; Peng, T.; Wei, B. *Appl. Surf. Sci.* **2013**, *270*, 238.
33. Cong, Y.; Long, M.; Cui, Z.; Li, X.; Dong, Z.; Yuan, G.; Zhang, J. *Appl. Surf. Sci.* **2013**, *282*, 400.
34. Qu, P.; Zhao, J.; Shen, T.; Hidaka, H. *J. Mol. Catal. A-Chem.* **1998**, *129*, 257.
35. Chala, S.; Wetchakun, K.; Phanichphant, S.; Inceesungvorn, B.; Wetchakun, N. *J. Alloy. Compd.* **2014**, *597*, 129.
36. Zhang, L.; Du, L.; Cai, X.; Yu, X.; Zhang, D.; Liang, L.; Yang, P.; Xing, X.; Mai, W.; Tan, S.; Gu, Y.; Song, J. *Physica E* **2013**, *47*, 279.
37. Xu, T.; Zhang, L.; Cheng, H.; Zhu, Y. *Appl. Catal. B-Environ.* **2011**, *101*, 382.